Piezoelectric-metal-magnet dc magnetoelectric sensor with high dynamic response

Long Zhang, Chung Ming Leung, Siu Wing Or, and S. L. Ho

Additional information on J. Appl. Phys.

Piezoelectric-metal-magnet dc magnetoelectric sensor with high dynamic response

Long Zhang, Chung Ming Leung, Siu Wing Or,[a)] and S. L. Ho
Department of Electrical Engineering, The Hong Kong Polytechnic University, Hung Hom, Kowloon, Hong Kong

A dc magnetoelectric sensor capable of measuring both dc and ac magnetic fields is developed by combining a thickness-polarized $0.7Pb(Mg_{1/3}Nb_{2/3})O_3$–$0.3PbTiO_3$ (PMN–PT) piezoelectric single-crystal plate, a pair of electrically connected aluminum strips, and a pair of NdFeB magnet plates in orthogonal directions. The operation of the sensor is based on the mechanical mediation of the magnetically biased Lorentz force effect in the aluminum strips due to a drive magnetic field (B_{3D}) applied to the sensor, a dc bias magnetic field (B_{3B}) preset by the NdFeB plates, and an ac reference electric current (I_2) flowing through the aluminum strips with the transverse piezoelectric effect in the PMN–PT plate at the sensor resonance. The theoretical and experimental results confirm an ultrahigh and linear current-controlled magnetic field sensitivity of 1.7 V/T/A in broad ranges of B_{3D} amplitude of -100 to $100\,mT$ and B_{3D} frequency of 0–15 kHz by using an I_2 of $\leq 100\,mA$ at the sensor resonance frequency of 65 kHz. © *2013 AIP Publishing LLC*. [http://dx.doi.org/10.1063/1.4812225]

I. INTRODUCTION

Magnetoelectric (ME) sensors have attracted considerable research and development attentions from scientists and engineers over the past decade because of their excellent potential in realizing passive sensing of magnetic fields in comparison with active sensing of magnetic fields in traditional Hall sensors.[1–4] The relatively sensitive ME sensors reported so far are mainly based on the extrinsic ME effect in magnetostrictive-piezoelectric composites, whereby an ac magnetic field applied to the composites induces an ac electric voltage through the product effect of the magnetostrictive and piezoelectric effects in the composites.[1–5] While the reported magnetostrictive-piezoelectric composite-based ME sensors generally exhibit magnetic field sensitivity and magnetic field range of linearity in excess of 100 V/T (or 10 mV/Oe) and 10 mT (or 100 Oe), respectively,[1–5] they are only well suited for sensing ac (or dynamic) magnetic fields rather than sensing dc/quasi-dc (or static/quasi-static) magnetic fields due to the decay of piezoelectric charges in the piezoelectric phase with time, especially for frequencies below 100 Hz.[6] This limitation significantly restricts the ME sensors to ac applications. In fact, the increasing demand for dc/quasi-dc magnetic field and electric current sensing of dc electric machines, dc power converters and drives, etc., in electric vehicles, intercity and high-speed rails, renewable energy systems, etc., has called for high-performance dc ME sensors with high dynamic responses.[7]

Recently, several studies have been performed to investigate the dc ME effect in magnetostrictive-piezoelectric composite plates, brass-piezoelectric composite disks, and aluminum-piezoelectric heterostructures based on the direct coupling of the Lorentz force effect in the magnetostrictive/brass/aluminum phase in response to a dc magnetic field

under an ac reference electric current with the piezoelectric effect in the piezoelectric phase.[8–10] Reasonably high and linear current-controlled dc magnetic field sensitivities ranging from 33 to 230 mV/T/A have been obtained for dc magnetic fields up to 180 mT under ac reference electric currents up to 300 mA amplitude and at 1 kHz frequency. However, neither ac nor quasi-dc response has been addressed in those studies; indeed, a lack of dynamic response data represent a bottleneck impeding further development.

In this paper, we report theoretically and experimentally a promising type of dc ME sensor having piezoelectric, metallic, and magnet phases arranged in orthogonal directions to induce the magnetically biased Lorentz force effect in the metallic phase under the support of the magnet phase and to couple the induced magnetically biased Lorentz force effect with the transverse piezoelectric effect in the piezoelectric phase, both at the resonance frequency of the sensor. The use of the magnetic biasing is to enable magnetic field sensing with phase information and to increase the output signal strength, while the operation of the sensor at resonance is to enhance the sensitivity and to broaden the operational frequency range. As a result, an interestingly high and linear current-controlled magnetic field sensitivity of 1.7 V/T/A, an extended magnetic field range of linearity of $\pm 100\,mT$, and a wide operational frequency range of 0–15 kHz are achieved.

II. STRUCTURE AND WORKING PRINCIPLE

Figure 1 illustrates the schematic diagram of the proposed three-phase piezoelectric-metal-magnet dc ME sensor in the Cartesian coordinate system. The sensor consisted of a $0.7Pb(Mg_{1/3}Nb_{2/3})O_3$–$0.3PbTiO_3$ (PMN–PT) piezoelectric single-crystal plate, a pair of electrically connected aluminum strips, and a pair of NdFeB magnet plates arranged orthogonally in the 1-, 2-, and 3-directions, respectively. In more details, the PMN–PT plate with its length along the
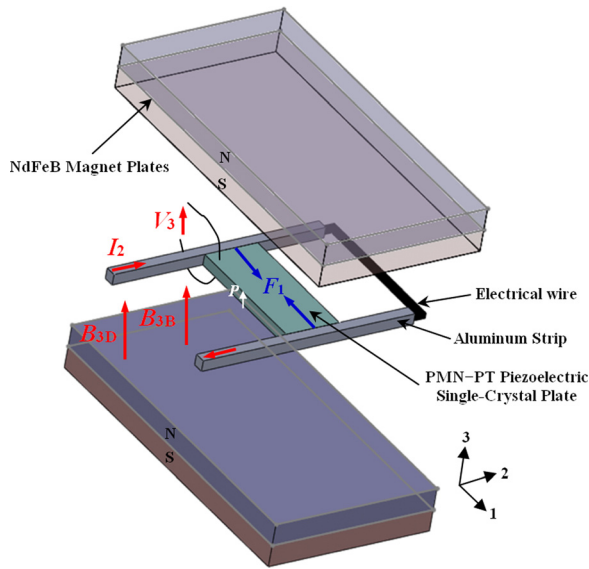
114, 027016-1

FIG. 1. Schematic diagram of the proposed three-phase piezoelectric-metal-magnet dc ME sensor in the Cartesian coordinate system.

1-direction was transversely bonded between the two electrically connected aluminum strips with their length along the 2-direction, and the whole piezoelectric-metal assembly was axially placed between the two NdFeB plates with their major surfaces normal to the 3-direction. The PMN−PT plate was supplied by Shanghai Institute of Ceramics, Chinese Academy of Sciences in China to have dimensions and crystallographic orientations of $14[100]^{L_P} \times 4[011]^{W_P} \times 1[0\bar{1}1]^{T_P}$ mm^3 (L_p: length, W_p: width, T_p: thickness), full fired silver electrodes on the two major surfaces perpendicular to the 3-direction, an electric polarization (P) along the 3- (or thickness) direction, a relative permittivity at constant stress ($\varepsilon_{33}^T/\varepsilon_0$) of 3900, a transverse piezoelectric voltage coefficient (g_{31}) of -50.6 mV m/N, a transverse electromechanical coupling coefficient (k_{31}) of 0.9, an elastic compliance coefficient at constant electric field (s_{11}^E) of 18.0 pN/m^2, and a density (ρ) of 8090 kg/m^3. The aluminum strips were prepared in-house by cutting a 1 mm thick 7075 aluminum sheet using an electrical discharge machining technique to give the desired length (L_s) of 20 mm and cross-sectional area of 1×1 mm^2. The NdFeB plates were acquired from China Rare Earth Magnet Ltd. to have dimensions of $30 \times 15 \times 2$ mm^3, a magnetization along the 3- (or thickness) direction, and nickel coating on their surfaces. In our sensor design, the NdFeB plates were situated axially with a spatial separation of 4 mm along the 3-direction so as to

create an average dc bias magnetic field (B_{3B}) of 100 mT for facilitating the effect of magnetically biased Lorentz force in the central aluminum strips to be further described in Secs. III–V.

The working principle of the dc ME sensor in Fig. 1 can be described as follows. Superimposing a drive magnetic field (B_{3D}) to be measured in the 3-direction on a dc bias magnetic field ($B_{3B} = 100$ mT in our case) preset by the NdFeB plates in the 3-direction under an ac reference electric current (I_2) flowing through the aluminum strips in the 2-direction at the resonance frequency (f_r) of the sensor results in a dc-biased attraction and repellent force (F_1) between the aluminum strips in the 1-direction due to the magnetically biased Lorentz force effect in accordance with Fleming's left hand rule.[11] Since the PMN–PT plate is transversely bonded between the aluminum strips, this F_1 will subsequently compress and extend the sandwiched PMN–PT plate in the 1-direction to generate an amplified ac piezoelectric voltage (V_3) across its thickness in the 3-direction at f_r owing to the resonance transverse piezoelectric effect.[12] The configuration and operation create two interesting characteristics for the sensor. First, the superimposition of a relatively small B_{3D} on a large B_{3B} ($=100$ mT) not only provides the phase information of B_{3D} but also enhances the strength of V_3. These suggest that V_3 has a nonzero constant amplitude at the frequency of a given I_2 (i.e., at f_r) even though B_{3D} vanishes. Second, the excitation of the sensor at its f_r, instead of at a nonresonance frequency (e.g., 1 kHz as used in the previous studies),[8–10] by I_2 can effectively enhance the sensitivity and broaden the operational frequency range.

To provide a quantitative description of the dynamic properties of the sensor, a dynamic magneto-mechano-electric equivalent circuit was constructed and is shown in Fig. 2. The magnetically biased Lorentz force effect in the aluminum strips and the NdFeB plates is modeled by a dc magnetic source (B_{3B}), an ac magnetic source (B_{3D}), and a current (I_2)-controlled magnetomechanical transformer (φ_m) according to the Lorentz force law as[11]

$$F_1 = (B_{3B} + B_{3D})L_s I_2, \qquad (1)$$

where $\varphi_m = L_s$ is the magnetomechanical transformation factor. The PMN–PT plate forced by F_1 and loaded with the aluminum strips is modeled as a three-port Mason model equivalent circuit in which φ_p and C_0 denote the mechano-electric transformation factor and clamped capacitance of the PMN–PT plate, respectively, while k_{eff} and Z_{eff} in the three acoustic impedances represent the effective wave
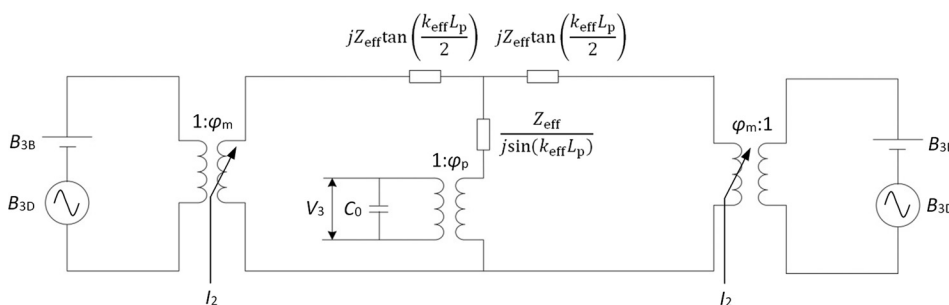

FIG. 2. Dynamic magneto-mechano-electric equivalent circuit of the sensor.

number and effective characteristic acoustic impedance of the PMN–PT plate loaded with the aluminum strips, respectively.[13] Physically, φ_p, C_0, k_{eff}, and Z_{eff} can be expressed as follows:

$$\varphi_p = \frac{W_p \varepsilon_{33}^T g_{31}}{s_{11}^E}, \tag{2}$$

$$C_0 = \frac{L_p W_p}{T_p} \varepsilon_{33}^T (1 - k_{31}^2), \tag{3}$$

$$k_{eff} = nk = n\omega\sqrt{\rho s_{11}^E}, \tag{4}$$

$$Z_{eff} = \rho \frac{\omega}{k_{eff}} W_p T_p = \frac{\rho W_p T_p}{n\sqrt{\rho s_{11}^E}}. \tag{5}$$

k_{eff} in Eqs. (4) and (5) states that the PMN–PT plate with wave number k is acoustically loaded by the aluminum strips so that the value of k is modified by a constant n (=0.69 in our case) to give k_{eff} and hence Z_{eff}. By solving Fig. 2 in terms of B_{3B}, B_{3D}, I_2, and V_3, the current-controlled magnetic field sensitivity (S) of the sensor is written as

$$S = \frac{\partial S_{I_2}}{\partial I_2} = \frac{\partial[\partial V_3/\partial(B_{3B} + B_{3D})]}{\partial I_2}$$

$$= -\frac{g_{31}\dfrac{L_s}{W_p}}{k_{31}^2 + (1 - k_{31}^2)\dfrac{k_{eff}L_p}{tan(k_{eff}L_p)}}, \tag{6}$$

where $S_{I_2} = \partial V_3/\partial(B_{3B} + B_{3D})$ is the magnetic field sensitivity at a given I_2. Equation (6) gives the following three noticeable cases: (1) In the absence of B_{3D}, V_3 still possesses a nonzero constant amplitude predefined by B_{3B} (=100 mT in our case) and I_2 at f_r; (2) In the presence of B_{3D} in form of an ac magnetic field, the resultant of B_{3B} and B_{3D} is a dc-biased ac magnetic field so that V_3 is an amplitude-modulated voltage signal with the amplitude and frequency of its envelope determined by those of $(B_{3B} + B_{3D})$ and B_{3D}, respectively, and the frequency of its carrier described by that of I_2; (3) In the presence of B_{3D} in form of a dc magnetic field, Eq. (6) can be reduced to

$$\lim_{f\to 0} S = -g_{31}\frac{L_s}{W_p}, \tag{7}$$

so that S of the sensor depends on g_{31} and W_p of the PMN-PT plate and L_s of the aluminum strips.

III. MEASUREMENTS

The static and dynamic properties of our proposed sensor were measured at room temperature by an in-house automated magnetoelectric measurement system.[5] B_{3D} of -100 to 100 mT dc was supplied by a water-cooled, U-shaped electromagnet (Myltem PEM-8005 K) under the control of a dc current supply (Sorensen DHP200-15) and the monitoring of a Hall probe connected to a gaussmeter (F. W. Bell 7030). B_{3D} of 1.5 mT peak in the frequency (f) range of

100 Hz$-$15 kHz was provided by a pair of Helmholtz coils driven by an arbitrary waveform generator (Agilent 33210 A) via a constant-current supply amplifier (AE Techron 7796HF). I_2 of 25–100 mA peak in the f range of 100 Hz$-$80 kHz was generated by the arbitrary waveform generator and amplified by the constant-current supply amplifier (AE Techron 7796HF). V_3 was determined by measuring the piezoelectric charge (Q_3) and capacitance (C) of the sensor using a charge meter (Kistler 5015 A) and a precision impedance analyzer (Agilent 4294 A), respectively, on the basis of the relation: $V_3 = Q_3/C$.

IV. RESULTS AND DISCUSSION

Figure 3 plots V_3 as functions of $(B_{3B} + B_{3D})$ in the range of $0-200$ mT and B_{3D} in the range of -100 to 100 mT dc at four different I_2 amplitudes of 25, 50, 75, and 100 mA peak and two different I_2 frequencies of 1 and 65 kHz. Since B_{3B} of 100 mT is preset in our work by the NdFeB plates, there is a shift of 100 mT between the upper and lower x-scales. For example, the data points of $(B_{3B} + B_{3D}) = 100$ mT correspond to those of $B_{3D} = 0$ mT. Nonetheless, V_3 shows good linear responses to both $(B_{3B} + B_{3D})$ and B_{3D} at different I_2 amplitudes and frequencies. It is recalled from Eq. (6) that S_{I_2} depends on the change in V_3 with respect to the change in $(B_{3B} + B_{3D})$ at a given I_2. S_{I_2} at a given I_2 is essentially the slope of each curve and can be obtained by a linear-fitting approach. At the sensor resonance frequency of 65 kHz, S_{I_2} is found to be 40.8, 88.0, 120.7, and 169.2 mV/T at $I_2 = 25$, 50, 75, and 100 mA peak, respectively. These values are almost seven times larger than those obtained at a nonresonance frequency of 1 kHz of 6.2, 13.5, 18.5, and 25.9 mV/T at $I_2 = 25$, 50, 75, and 100 mA peak, respectively.

Figure 4 shows the dependence of S_{I_2} on I_2 at 1 and 65 kHz. The values of S_{I_2} are extracted from Fig. 3 as discussed. It is clear that S_{I_2} increases linearly with an increase in I_2 at both 1 and 65 kHz. This indicates the presence of a high and linear controllability of S_{I_2} in the sensor by I_2.
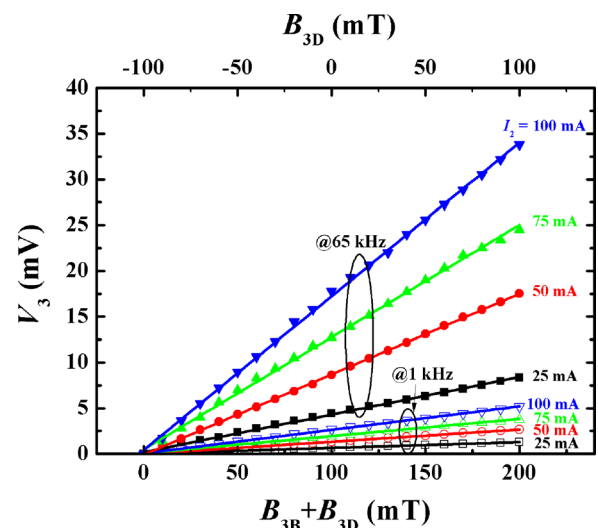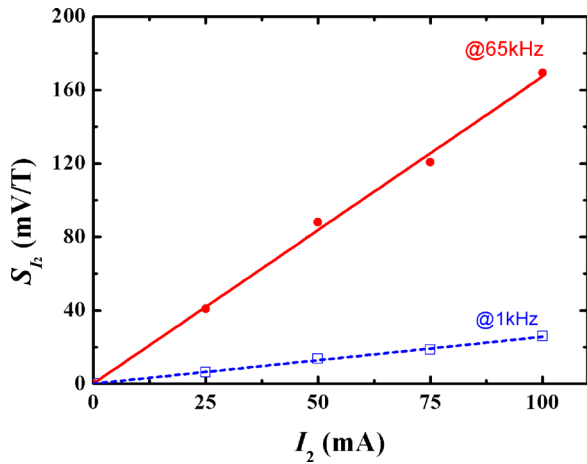

FIG. 3. V_3 as functions of $(B_{3B} + B_{3D})$ in the range of 0–200 mT and B_{3D} in the range of -100 to 100 mT dc at four different I_2 amplitudes of 25, 50, 75, and 100 mA peak and two different I_2 frequencies of 1 and 65 kHz.

FIG. 4. Dependence of S_{I_2} on I_2 at 1 and 65 kHz.

Based on the expression of S in Eq. (6), and by linear fitting the S_{I_2}–I_2 curves in Fig. 4, S of our sensor is found to be 0.26 and 1.7 V/T/A at 1 and 65 kHz, respectively. S obtained at the sensor resonance frequency of 65 kHz is approximately seven times enhanced compared with that acquired at a non-resonance frequency of 1 kHz.

Figure 5(a) illustrates the waveforms of V_3 in response to three different B_{3D} of 50, 0, and −50 mT dc at an I_2 of 50 mA peak amplitude and 1 kHz frequency, while Fig. 5(b) gives the waveforms at a different I_2 frequency of 65 kHz. At both I_2 frequencies, V_3 is essentially clean and does not show any amplitude offset and phase shift. This suggests the
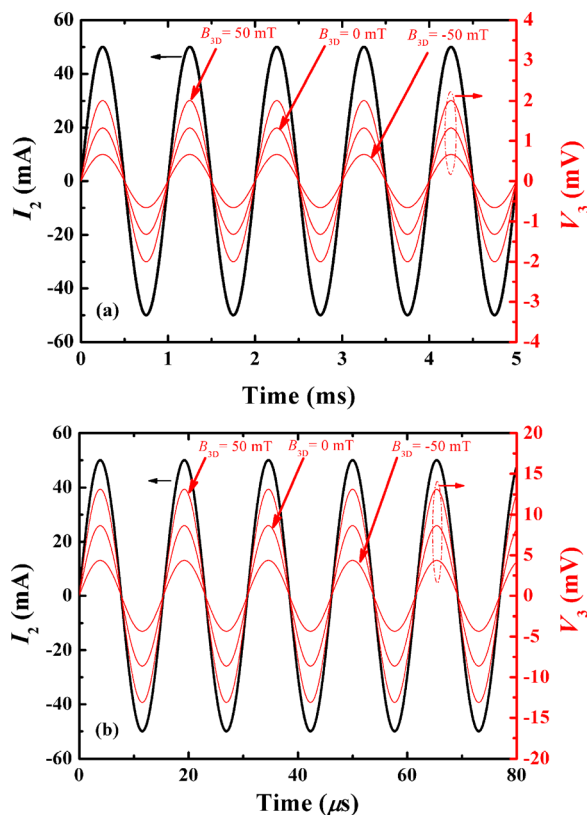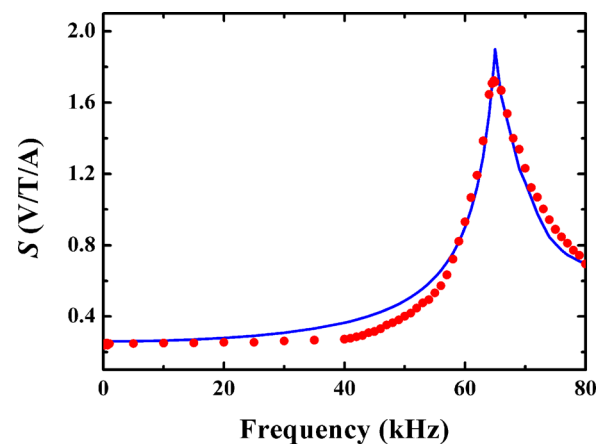
existence of a stable mediation of the magnetically biased Lorentz force effect with the transverse piezoelectric effect in the sensor. In Fig. 5(a), the sensor referenced at an I_2 of 50 mA peak amplitude and 1 kHz frequency is capable of producing a nonzero V_3 of 1.32 mV peak amplitude and 1 kHz frequency even though B_{3D} is 0 mT. At a positively elevated B_{3D} of 50 mT dc and a negatively elevated B_{3D} of −50 mT dc, an enhanced V_3 of 2.00 mV peak and a reduced V_3 of 0.66 mV peak are produced at 1 kHz, respectively. In Fig. 5(b), obviously improved signal strength and sensitivity are observed when the sensor is referenced at its resonance frequency of 65 kHz. Enhanced V_3 of 12.85, 8.46, and 4.26 mV peaks is recorded at 65 kHz in response to an applied B_{3D} of 50, 0, and −50 mT dc, respectively.

Figure 6 shows the calculated and measured S spectra of the sensor. The S spectrum obtained from calculation in accordance with Eq. (6) agrees reasonably well with that acquired from measurement with a swept sinusoidal I_2 of 50 mA peak in the frequency range of 0–80 kHz. In both spectra, the sensor demonstrates an essentially flat response for frequencies up to 20 kHz (i.e., the nonresonance region) with a high S of about 0.26 V/T/A. At the sensor resonance frequency of 65 kHz, an ultrahigh S of 1.89 V/T/A is deduced by calculation and of 1.7 V/T/A is observed by measurement. This measured resonance S (=1.7 V/T/A) not only coincides well the results described in Figs. 3–5 but also confirms the effectiveness of enhancing S by referencing the sensor at its resonance frequency by I_2.

Figure 7 displays the waveforms of V_3 and $(B_{3B} + B_{3D})$ for B_{3B} of 100 mT, B_{3D} of 1.5 mT peak amplitude and 100 Hz frequency, and I_2 of 50 mA peak amplitude and 65 kHz frequency. In response to the dc-biased ac magnetic field $(B_{3B} + B_{3D})$, the resulting V_3 is in form of an amplitude-modulated voltage signal in which the amplitude of $(B_{3B} + B_{3D})$ and the frequency of B_{3D} (i.e., 100 Hz) determine the amplitude and frequency of the envelope, respectively, while the frequency of I_2 (i.e., 65 kHz) controls that of the carrier.

In order to evaluate the response of the sensor to different B_{3D} frequencies so as to determine the operational frequency range of the sensor, Fig. 8 shows the waveforms of V_3 and $(B_{3B} + B_{3D})$ for four different B_{3D} frequencies of 1, 5,

FIG. 5. Waveforms of V_3 in response to three different B_{3D} of 50, 0, and −50 mT dc at an I_2 of 50 mA peak amplitude and (a) 1 and (b) 65 kHz frequency.

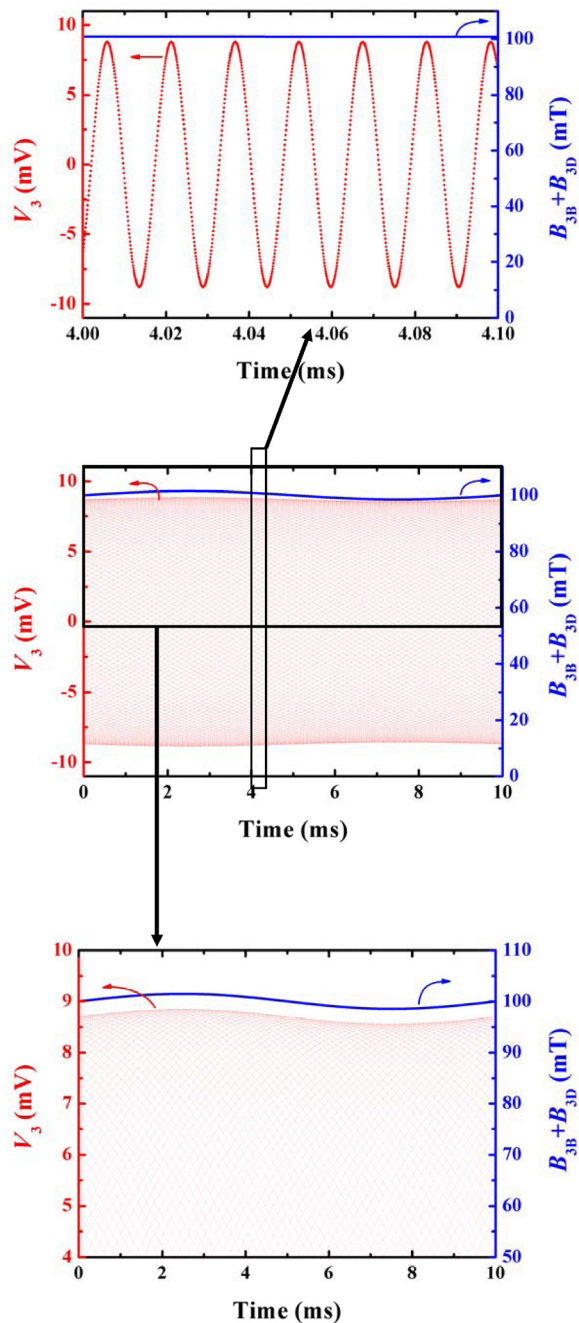FIG. 6. Calculated (line) and measured (symbol) S spectra of the sensor.

FIG. 7. Waveforms of V_3 and $(B_{3B} + B_{3D})$ for B_{3B} of 100 mT, B_{3D} of 1.5 mT peak amplitude and 100 Hz frequency, and I_2 of 50 mA peak amplitude and 65 kHz frequency.

10, and 15 kHz at given B_{3B} of 100 mT, B_{3D} of 1.5 mT peak, and I_2 of 50 mA peak amplitude and 65 kHz frequency. Agreed with the observation in Fig. 7, V_3 delivers an amplitude-modulated voltage signal with its envelope and carrier frequencies follow the B_{3D} and I_2 frequencies, respectively. It is important to note that when the B_{3D} frequency is well below the I_2 frequency of 65 kHz (e.g., B_{3D} at 100 Hz in Fig. 7), the waveform of V_3 can be precisely constructed in accordance with that of B_{3D}. The quality of the waveform decreases with increasing B_{3D} frequency as can be seen clearly from Fig. 8. If the B_{3D} frequency is elevated to 15 kHz, the waveform quality becomes marginal [Fig. 8(d)]. This suggests that our sensor has a broad operational
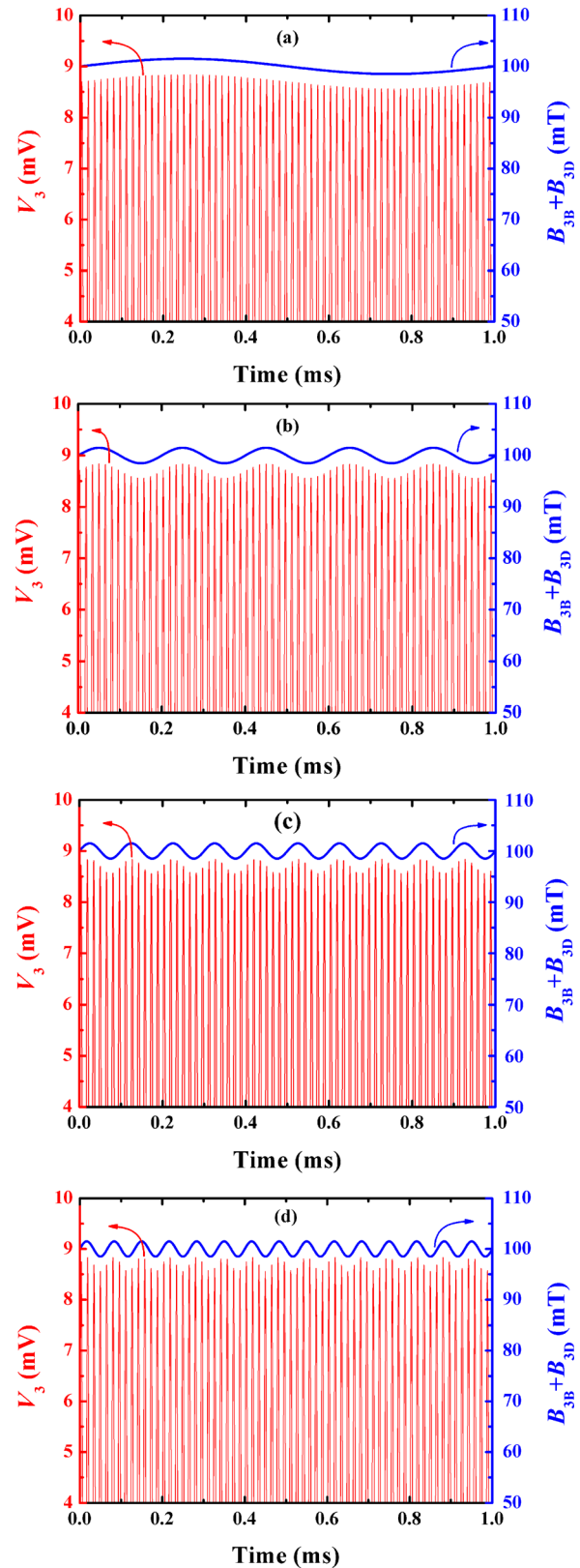

FIG. 8. Waveforms of V_3 and $(B_{3B} + B_{3D})$ for four different B_{3D} frequencies of (a) 1, (b) 5, (c) 10, and (d) 15 kHz at given B_{3B} of 100 mT, B_{3D} of 1.5 mT peak, and I_2 of 50 mA peak amplitude and 65 kHz frequency.

frequency range from 0 to about 15 kHz. In addition, the frequency limit of 15 kHz is about one fourth of the resonance frequency of 65 kHz, which is in agreement with the 4-times frequency requirement as stated by the sampling theorem.[14]

V. CONCLUSION

We have developed a three-phase piezoelectric-metal-magnet dc ME sensor based on the mechanical mediation of the magnetically biased Lorentz force effect with the transverse piezoelectric effect, both operating at the resonance frequency of the sensor. We have also reported theoretically and experimentally the static and dynamic properties of the sensor. The results have demonstrated an ultrahigh and linear current-controlled magnetic field sensitivity of 1.7 V/T/A, an extended magnetic field range of linearity of ± 100 mT, and a wide operational frequency range of 0–15 kHz by using a reference electric current of ≤ 100 mA at the sensor resonance frequency of 65 kHz. The maximum operational frequency of 15 kHz has been found to obey the 4-times frequency requirement as stated by the sampling theorem. The ability of the sensor to sense both dc and ac magnetic fields with high dynamic response has opened up a new direction in the research, development, and applications of ME materials and sensors.

ACKNOWLEDGMENTS

[1]M. Fiebig, J. Phys. D **38**, R123 (2005).

[2]S. Priya, R. Islam, S. X. Dong, and D. Viehland, J. Electroceram. **19**, 149 (2007).

[3]C. M. Leung, S. W. Or, S. Y. Zhang, and S. L. Ho, J. Appl. Phys. **107**, 09D918 (2010).

[4]Y. J. Chen, S. M. Gillette, T. Fitchorov, L. P. Jiang, H. B. Hao, J. H. Li, X. X. Gao, A. Geiler, C. Vittoria, and V. G. Harris, Appl. Phys. Lett. **99**, 042505 (2011).

[5]Y. M. Jia, S. W. Or, J. Wang, H. L. W. Chan, H. L. W. Chan, X. Y. Zhao, and H. S. Luo, J. Appl. Phys. **101**, 104103 (2007).

[6]M. Blejan, I. Ilie, B. Lupu, and M. Comes, in *Proceedings of the 31st International Spring Seminar on Electronics Technology*, (2008), p. 343.

[7]R. Roll and K. J. Overshott, *Sensors: Magnetic Sensors* (Wiley Online Library, 2008), Vol. 5.

[8]Y. M. Jia, Y. X. Tang, X. Y. Zhao, H. S. Luo, S. W. Or, and H. L. W. Chan, J. Appl. Phys. **100**, 126102 (2006).

[9]Y. M. Jia, D. Zhou, L. H. Luo, X. Y. Zhao, H. S. Luo, S. W. Or, and H. L. W. Chan, Appl. Phys. A **89**, 1025 (2007).

[10]C. M. Leung, S. W. Or, and S. L. Ho, J. Appl. Phys. **107**, 09E702 (2010).

[11]R. F. Harrington, *Introduction to Electromagnetic Engineering* (McGraw-Hill, Mineola, NY, 2003).

[12]T. Ikeda, *Fundamentals of Piezoelectricity* (Oxford University Press, Oxford, 1990).

[13]B. A. Auld, *Acoustic Fields and Waves in Solids* (R. E. Krieger, Malabar, Florida, 1990).

[14]S. W. Smith, *The Scientist and Engineer's Guide to Digital Signal Processing* (California Technical Publishing, 1997).